Multiuser Visible Light Communication Systems Using OFDMA

Jie Lian, *Member, IEEE*, and Maïté Brandt-Pearce, *Senior Member, IEEE*

(ECOC 2019-Invited Paper)

***Abstract*—Visible light communications (VLC), a short-range optical wireless communication scheme using light-emitting diodes (LEDs) as transmitters, has been proposed to support multiple users, predominantly in indoor environments. This article explores using orthogonal frequency division multiple access (OFDMA) for VLC due to its high spectrum utilization efficiency and potentially high transmission data rate. The proposed optical OFDMA uses adjacent subcarriers as a set to support each user. Doing so allows some users to sample at a lower sampling rate and employ a smaller fast Fourier transform (FFT) to lower the computational complexity and hardware cost. A multi-cell structure is naturally obtained in VLC since more than one LED lamp is usually installed in an indoor environment. In this article, users located in different cells can reuse the same subcarrier sets, potentially causing multiple access interference. Analysis and simulation results are used to predict the subcarrier-set reuse probability over the entire indoor space. When the OFDM modulation index is optimized considering the peak-power-limit of the LEDs, the average transmission data rate is twice that of using OFDM that does not reuse the spectral resources, for the scenarios tested.**

***Index Terms*—Multiple access, OFDMA, optical OFDM, visible light communications.**

I. Introduction

VISIBLE light communications (VLC) using light-emitting diodes (LEDs) as transmitters is a short-range communication technique that has attracted the attention of academic and industry researchers in the last ten years [1], [2]. Due to its advantages over radio frequency (RF) communications, such as the lack of spectrum regulation, low electromagnetic interference, low power consumption, and high security, VLC has become an attractive candidate technology to support high-speed indoor connections for 5G and Internet of things (IoT) applications. LEDs working as lighting devices are widely deployed, potentially providing a promising market for VLC systems [3]. Since non-coherent light is emitted from the LEDs, intensity modulation and direct detection (IM/DD) should be used, requiring a targeted modulation and multiple access scheme design [4].

The capability of providing multiple access with reliable high data rate is a critical criterion to evaluate the performance of a communication system. When multiple LEDs are employed in a cellular structure, a high density of users with high data transmission rates in indoor applications is possible using VLC [5]. Optical multiple access schemes can generally be classified as single-carrier or multi-carrier. Time division multiple access (TDMA) and code division multiple access (CDMA) are typical single-carrier schemes applied in VLC systems [6], [7]. CDMA requires orthogonal codewords to separate users; since IM/DD is used in VLC systems, the optical CDMA codewords are not fully orthogonal, causing multiple access interference (MAI). Orthogonal frequency division multiple access (OFDMA) is a multi-carrier scheme that was originally proposed in RF systems for frequency-selective channels. In VLC systems, optical OFDMA is a promising candidate scheme to support multiple users with high data rates by transmitting spectrally-efficient orthogonal frequency-division multiplexed (OFDM) signals [8], [9]. OFDM can reduce inter-symbol interference (ISI) caused by the bandlimited channel due to the LED's slow rise-time. This modulation has therefore been extensively applied in VLC systems to improve the data rate. The spatial information of users dispersed in the room can also be exploited to enhance the multiple access performance. Space division multiple access (SDMA) is often combined with other multiple access schemes. [10].

Cellular access structures designed for telecommunication systems are powerful for supporting multiple users. Due to the limited illumination reach of lighting fixtures, cells are naturally built based on the existing lighting infrastructure. A testbed for multi-cell VLC systems was built and described in [11]. The signal to noise ratio (SNR) within the cells was measured, and a handover scheme and its performance were reported. For a multi-cell indoor VLC system, inter-cell interference needs to be considered and mitigated. [12] proposes a jointly designed precoder and equalizer to combat inter-cell interference and thus support multiple users. Soft frequency reuse is another method to mitigate inter-cell interference. In [13], a specifically designed LED lamp with two fields-of-view (FOVs) is used to separate a cell into two components, each of which uses a specific frequency so that it can be reused in different cells. The OFDMA research described in [14] and [15] includes power allocation and

Manuscript received December 10, 2019; revised March 3, 2020, April 29, 2020, and June 6, 2020; accepted June 29, 2020. Date of publication July 9, 2020; date of current version November 1, 2020. This work was supported in part by the Fundamental Research Funds for the Central Universities under Grant 3102020HHZY030002 *(Corresponding author: Jie Lian.)*

Jie Lian is with the School of Marine Science and Technology, Northwestern Polytechnical University, Xi'an 710072, China (e-mail: jielian@nwpu.edu.cn).

Maïté Brandt-Pearce is with the Charles L. Brown Department of Electrical and Computer Engineering, University of Virginia, Charlottesville, VA 22904 USA (e-mail: mb-p@virginia.edu).

Color versions of one or more of the figures in this article are available online at https://ieeexplore.ieee.org.

Digital Object Identifier 10.1109/JLT.2020.3008290

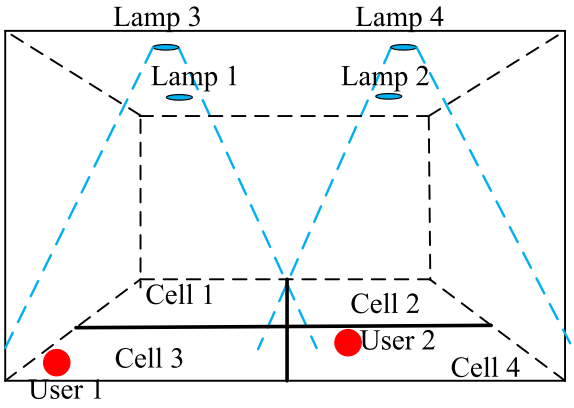

Fig. 1. Illustration of a cell structure in VLC systems.

subcarrier allocation algorithms, respectively, for multiple users in VLC systems. Although [14] considers a multi-cell structure in an indoor environment, subcarriers and frequency reuse are not taken into account. [15] uses DCO-OFDM, as do we, but the peak radiation power constraint of LEDs is not modeled.

We recently proposed a multiuser VLC system based on OFDMA [16], where a multi-cell structure is used to support a high density of users. In this paper, we expand on this idea. In traditional OFDMA systems, a high sampling rate and bandwidth are required due to the large fast Fourier transform (FFT) needed. Many IoT devices, however, are unable to sample at such high rates. In our work, adjacent subcarriers are used as a set assigned to a user for transmission. At the receiver, users assigned a low-frequency subcarrier set may be able to use a slower sampling rate and a smaller FFT to demodulate the signal, simplifying the receiver structure. Therefore, the bandwidth requirement at the receiver of some users can be smaller than using traditional OFDMA, which is attractive for IoT systems. In addition, with clever resource allocation across the multi-cell structure, the OFDMA frequency subcarrier sets can be reused in different cells, increasing the system throughput. The main contribution of this paper is that it comprehensively considers power allocation, subcarriers allocation, frequency reuse, sampling rate reduction, and clipping distortion in OFDM for multiuser indoor VLC systems.

The remainder of the paper is organized as follows. Section II describes the multiuser VLC system. The principles of the proposed OFDMA are presented in Section III. Numerical results are discussed in Section IV. Finally, the paper is concluded in Section V.

II. Multiuser VLC System

In this section, the multiuser VLC system is described, which includes the multi-cell structure and indoor VLC channel model.

A. Multi-Cell Structure

Cellular networks were originally designed to support multiple users in RF systems. In fact, the success of 5G is predicated on the formation of small cells, which occur naturally in indoor VLC systems since lamps illuminate a small area Fig. 1 illustrates an indoor cellular network for a VLC system. In this figure, four LED lamps function as lighting devices and simultaneously support multiple users. Since each LED lamp typically has a large illumination area (parts of which may be quite dim), we artificially define the access area of the cell, that we simply call the *cell*, which is often smaller than the illumination area. In this paper, each user is served only by one LED lamp, and thus a cell is defined as the portions of the room that receive the strongest light power from that lamp, compared with other VLC transmitters. Each cell only contains a single VLC-enabled LED lamp, and each lamp only serves the users within its cell. The cells are non-overlapping, which often leads to a square or hexagonal tessellation. For example, in Fig. 1, square cells are created based on the locations of the LEDs. User 1 is located in cell 3 and is thus served by lamp 3, while user 2 is connected to lamp 4. With the help of a multi-cell structure, the frequency resources can be reused, as in RF systems [17].

B. Channel Model

In a typical VLC system, white lighting LEDs are used for illumination and downlink communications. Commonly-used lighting LEDs are bandlimited due to their slow rise-time, the 3 dB bandwidth of which is usually limited to a few tens of MHz [18]. The light emitted is reflected from walls, obstacles, and other reflecting surfaces, which results in a dispersive indoor VLC channel. The overall bandwidth of the system is often dominated by the LED response because of its strong bandwidth limitation.

The channel loss is determined by the transmission link geometry and the LED's beamwidth, based on the Lambertian law, and can be represented as [19]

$$g = \frac{A\cos\phi}{2\pi d^2}(m+1)\cos^m\psi, \tag{1}$$

where ϕ is the photodetector (PD) incidence angle and ψ is the LED radiation angle. m is the Lambertian mode that is related to the LED beamwidth. d and A are the propagation distance and the effective area of the receiver's PD, respectively. Considering the strong bandwidth limitation of LEDs, in this work the system response including the transmitter and channel is modeled as a first order low-pass filter with normalized impulse response called $h(t)$ [20]. Thus, the impulse response from LED q to the input of the kth user's receiver is modeled as $g_{qk}h(t)$, where g_{qk} is the corresponding channel loss derived using (1) based on the location of the lamp and user.

III. Principles of Proposed OFDMA Scheme

In this section, the proposed downlink OFDMA scheme employing the multi-cell structure given in Section II-A to support multiple users is described. Transmitted and received signal models, as well as the subcarrier reuse scheme, are presented and discussed.

OFDM has recently gained popularity for VLC systems. Since IM/DD must be used, only positive and real-valued OFDM signals can be transmitted. Many modifications of traditional

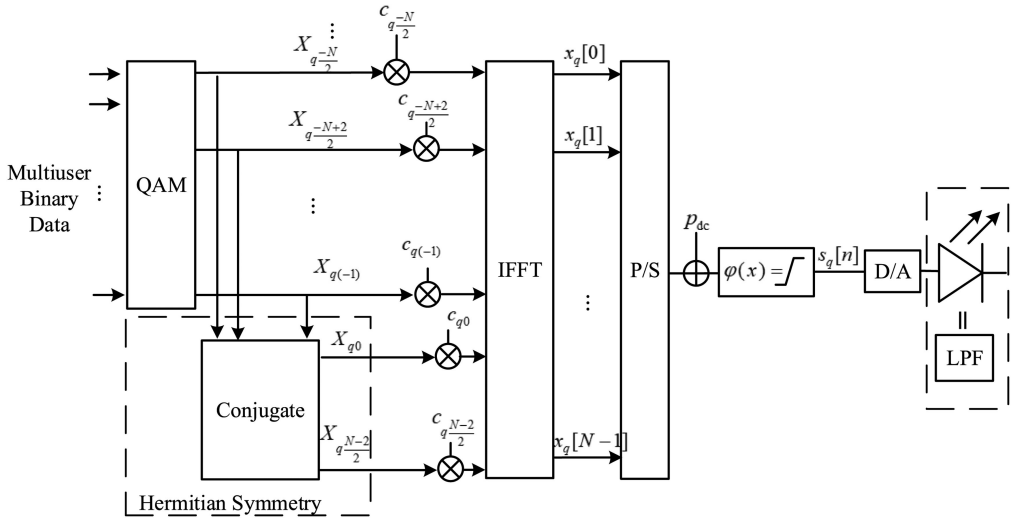

Fig. 2. Block diagram of the multiuser OFDMA system, (b) subcarriers in the proposed OFDMA system.

RF OFDM to satisfy these constraints, jointly called *optical OFDM*, have been proposed, such as DC-biased optical OFDM (DCO-OFDM), asymmetrically clipped optical OFDM (ACO-OFDM), Flip-OFDM, and clipping-enhanced optical OFDM (CEO-OFDM) [21]–[24]. DCO-OFDM is the most common optical OFDM scheme used in VLC systems. The focus of this paper is not to minimize clipping distortion caused by the LED's nonlinearity when optical OFDM is applied, as many of these schemes do, but rather on the resource allocation and reuse issue. Any optical OFDM schemes can be employed to support multiple users in the proposed system. For simplicity, we restrict our analysis to DCO-OFDM for data transmission.

A. Transmitted Signal

The transmitted downlink signal is a standard DCO-OFDM signal. We improve upon this basic modulation scheme by optimizing the power allocation across subcarriers while considering the peak radiation power constraint.

A block diagram of the proposed OFDMA transmitter for K users sharing N subcarriers is provided in Fig. 2. To simplify the notation in the figure and subsequent equations, we model the signal in only one OFDM symbol, assuming a standard cyclic prefix would be adopted in any implementation to avoid ISI. The binary data for each user is first modulated using M-ary quadratic amplitude modulation (M-QAM). Note that, since baseband IM/DD is used in VLC systems, the data input to the inverse fast Fourier transform (IFFT) should have Hermitian symmetry to ensure that the output signal is real-valued. A bipolar OFDM signal is generated by the IFFT in LED q, which can be modeled as

$$x_q[n] = \frac{1}{N}\sum_{\ell=-N/2}^{N/2-1} c_{q\ell} X_{q\ell} \exp\{j2\pi n\ell/N\} \quad n = 0, 1, \ldots, N-1, \tag{2}$$

where $X_{q\ell}$ is the M-QAM data for the ℓth subcarrier in cell q. $X_{q\ell}$ and $X_{q(-\ell-1)}$ are Hermitian pairs, generated using the conjugate function as shown in Fig. 2$c_{q\ell}$ represents the modulation index that controls the scale of the signal $X_{q\ell}$. In this paper, we optimize this modulation index to maximize the throughput.

With the help of the central limit theorem, $x_q[n]$ can be approximately modeled as a Gaussian distributed random variable with zero mean. The variance of $x_q[n]$ is $\sigma_{x,q}^2 = \frac{2\sigma_d^2}{N^2}\sum_{\ell=0}^{N/2-1} c_{q\ell}^2$, where σ_d^2 is the variance of $X_{q\ell}$, assumed equal $\forall\, q$, and ℓ.

To avoid transmitting negative signals, a constant DC bias is added to $x_q[n]$, turning the OFDM signal into a DCO-OFDM signal. Then, the nth sample of the signal for LED q can be written as

$$s_q[n] = \varphi\left(x_q[n] + P_{\mathrm{dc}}\right),\ n = 0, 1, \ldots, N-1, \tag{3}$$

where $\varphi(x)$ represents the nonlinear LED transfer function, which is modeled as a piece-wise function given as

$$\varphi(x) = \begin{cases} P_{\max}, & x \geq P_{\max} \\ x, & 0 < x < P_{\max} \\ 0, & x \leq 0 \end{cases}. \tag{4}$$

$P_{\max}$ represents the peak radiation power of the LEDs. Time samples of the signal that have a magnitude beyond this power constraint must be hard clipped, introducing clipping distortion. P_{dc} is the DC power added, which is usually set to $P_{\max}/2$ to account for both the zero and peak power constraints. The signal $s_q[n]$ convolved with a low-pass filter (LPF in Fig. 2) to account for the LED bandlimit is then emitted as optical power.

After adding the DC bias to $x_q[n]$, the probability density function (pdf) of $x_q[n] + P_{\mathrm{dc}}$, $f_q(x)$, is that of a Gaussian random variable with mean P_{dc} and variance $\sigma_{x,q}^2$.

B. Received Signal

In traditional RF communications, OFDMA is often used in frequency selective channels, where subcarriers may be assigned

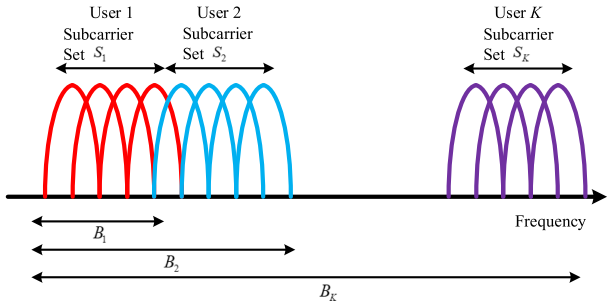

Fig. 3. Subcarrier allocation in the proposed OFDMA system.

to a user to avoid multipath fading or other interference. The entire spectral band is downconverted and sampled using the same sampling rate, and then demodulated using the same N-FFT [25, Ch.5]. In traditional VLC OFDMA, all users employ the same sampling rate and N-FFT as well; the signal is baseband, so there is no downconversion. We want to accommodate a few IoT users that may have relatively low processing speeds and computational resources, and thus a lower sampling rate. The proposed IM/DD OFDMA spectrum allocation shown in Fig. 3 uses adjacent subcarriers to modulate the data for each user. Based on the user's hardware capability, the bandwidth used for user k, labeled B_k, could be lower than the entire bandwidth used in traditional OFDMA systems, depending on which subcarrier subset is assigned to the user; we show in this section how such users can employ a lower sampling rate and a smaller FFT, leading to a simpler receiver's structure. Note that if all the users in a cell have tight bandwidth constraints, the low frequency subcarriers must be shared.

In this section, the received signal is modeled and analyzed based on the receiver sampling rate. We define the subcarriers used for user k in one cell as a subcarrier set, S_k, as illustrated in Fig. 3. The size of S_k is denoted as $|S_k|$; therefore, $\sum_{k=1}^{K}|S_k| = \frac{N}{2}$. Fig. 4 shows a block diagram of the receivers, where the signal received at the kth user is filtered with its corresponding bandwidth, B_k. Let the users be sorted in an ascending order of B_k in each cell. We assume $2N_k$ represents the size of the FFT for user k, where N_k, which should be a power of 2, is calculated by

$$N_k = 2^{\lceil \log_2\left(\sum_{j=1}^{k}|S_j|\right)\rceil}, \tag{5}$$

where $\lceil x \rceil$ represents the least integer greater than or equal to x. Therefore, the bandwidth of user k's anti-aliasing filter becomes $B_k = N_k R_s$, where R_s is the transmitted OFDM symbol rate. After low-pass filtering, the sampling rate of $2N_k R_s$ may be employed by user k's receiver. Adjacent channel interference and aliasing from the subcarrier near the filter cutoff frequency may be introduced if the filter is not sufficiently sharp. For the analysis in this paper, we assume the receiver filters used are sharp enough to suppress the adjacent subcarriers so that the interference caused by imperfect filtering can be neglected. This assumption is validated via simulation in Section IV. In cases where a sharp filter cannot be employed, the subcarrier near the transition band of the filter may become unusable and should remain unmodulated to avoid aliasing and interference.

After low-pass filtering, removing the DC, and sampling the received signal at a rate of $2N_k R_s$, we represent the nth sample of the received signal at user k in cell q as

$$r_{qk}[n] = \rho \cdot h_{qk}[n] * (\alpha_q \cdot x_q[n] + w_{\text{clip},q}[n]) + w_k[n], \tag{6}$$

where $h_{qk}[n]$ represents the nth sample of the discrete-time version of the end-to-end channel impulse response from LED q to the kth user including the LED impulse response $h(t)$ and channel gain g_{qk} [from Section II-B]. ρ represents the PD responsivity, $*$ represents discrete-time convolution, and α_q is the clipping coefficient that accounts for the power loss from the nonlinear clipping due to the peak radiation power constraint on the LED of lamp q [26]. $w_{\text{clip},q}[n]$ represents the nth sample of the clipping noise that is caused by the signal clipping at zero and the peak power at LED q, which is modeled as a Gaussian random variable with zero mean. $w_k[n]$ is the nth sample of the additive Gaussian noise at the receiver of user k after the low-pass filter, which combines the shot and thermal noises.

At the receiver, a single-tap equalizer is needed to counter the phase distortion due to the dispersive the channel. Then, an estimate of the intended M-QAM data modulated on the ℓth subcarrier in the qth cell, after the $2N_k$-FFT demodulation operation at user k, can be modeled as

$$\hat{X}_{q\ell} = \alpha_q \rho \frac{2N_k}{N}|H_{qk}[\ell]|c_{q\ell}X_{q\ell} + W_{\text{clip},q}[\ell] + W_k[\ell], \tag{7}$$

where user k served by cell q is assigned subcarrier ℓ. $\frac{2N_k}{N}$ represents a signal amplitude loss due to the use of an FFT of size $2N_k$ instead of N. $W_{\text{clip},q}[\ell]$ and $W_k[\ell]$ are the effective clipping noise and additive noise at the ℓth subcarrier after the $2N_k$-FFT at the receiver. $H_{qk}[\ell]$ represents the channel gain for subcarrier ℓ of user k in the qth cell, where $\ell = 0, 1, \ldots, N_k - 1$. The derivation of (7) can be found in the Appendix.

The clipping loss coefficient shown in (7) can be calculated based on the Bussgang theorem [27] as

$$\begin{aligned}\alpha_q &= \frac{1}{\sigma_{x,q}^3\sqrt{2\pi}}\int_{-\infty}^{\infty} x\varphi(x)\exp\left(-\frac{(x-P_{\text{dc}})^2}{2\sigma_{x,q}^2}\right)dx \\ &= 1-\frac{1}{2}\Bigg(\text{erfc}\left(\frac{-\sqrt{\sum_{\ell=0}^{N/2-1}c_{q\ell}^2}+\sqrt{2}P_{\max}N}{2\sqrt{\sum_{\ell=0}^{N/2-1}c_{q\ell}^2\sigma_d^2}}\right) \\ &\quad + \text{erfc}\left(\frac{\sqrt{\sum_{\ell=0}^{N/2-1}c_{q\ell}^2}+\sqrt{2}P_{\max}N}{2\sqrt{\sum_{\ell=0}^{N/2-1}c_{q\ell}^2\sigma_d^2}}\right)\Bigg).\end{aligned} \tag{8}$$

Since the additive receiver noise $w_{\text{k}}[n]$ is assumed to be white and Gaussian, the variance of $W_k[\ell]$ can be calculated as $\frac{B_k}{2N_k}\mathcal{N}_o$, where $\mathcal{N}_o$ represents the noise spectral density. The variance of $W_{\text{clip},q}[\ell]$ is $\frac{4N_k^2}{N}\sigma_{\text{clip},q}^2$, where $\sigma_{\text{clip},q}^2$ is the variance of the clipping noise $w_{\text{clip},q}[n]$ sampled at the full rate, NR_s. $\sigma_{\text{clip},q}^2$ can be calculated as [24], [28]

$$\sigma_{\text{clip},q}^2 = \int_{-\infty}^{0} x^2 f_q(x)dx + \int_{P_{\max}}^{\infty} x^2 f_q(x)dx. \tag{9}$$

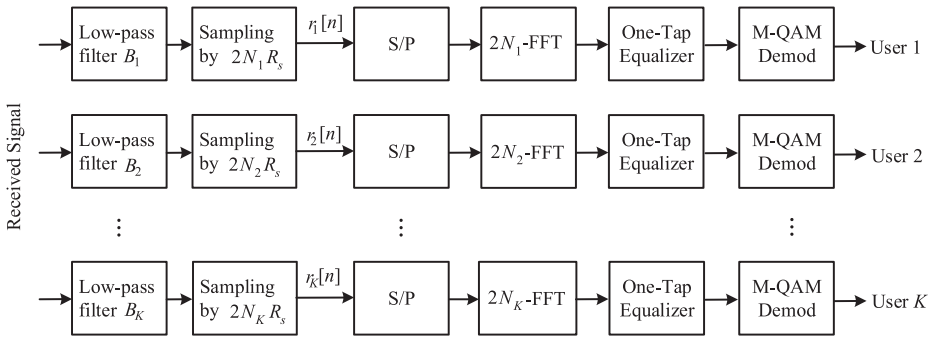

Fig. 4. Block diagram of the VLC receivers.

TABLE I
AN EXAMPLE OF THE SUBCARRIERS USAGE AND THE CORRESPONDING FFT SIZE

Users	User 1	User 2	User 3
Number of assigned subcarriers	2	5	8
Index of the assigned subcarriers	0-1	2-7	8-15
Size of FFT	4-FFT	16-FFT	32-FFT

Table I shows an example to illustrate the number of assigned subcarriers for the users and their corresponding FFT sizes for a system using $N = 32$. User 1 is assigned two subcarriers, $\ell = 0$ and 1; it can thus use a 4-FFT for demodulation due to the requisite Hermitian symmetry. For user 1, a sampling rate 8 times lower is required than if it had been assigned higher-frequency subcarriers. For user 2, although 5 subcarriers are assigned, a 16-FFT is needed since its subcarrier set includes subcarrier 7. Similarly, a full 32-FFT is used at the receiver of user 3 because the highest 8 subcarriers are assigned.

C. Subcarrier Set Reuse

As described above, users in the same cell may be served using different subcarrier sets. With the help of the multi-cell structure described in Section II-A, the subcarrier sets can potentially be reused in different cells. This section introduces and analyses the subcarrier reuse scenario.

MAI caused by signals transmitted using the reused subcarrier sets degrades the system performance, which diminishes the achievable throughput. When the SINR of a subcarrier is severely impacted by MAI, it cannot be used. Fig. 5(a) illustrates the subcarriers set reuse scheme for systems using two frequency sets (high and low). In cell 1 supported by lamp 1, users 1 and 2 utilize the low and high-frequency subcarrier sets, respectively. In cell 2, the same low and high-frequency subcarrier sets are reused by users 3 and 4. Two examples, illustrated in Fig. 5(b), show scenarios in which subcarrier reuse can and cannot be applied. In both examples, four active users are served by two lamps. In the figure, the channel loss between lamp q and the unintended user k, g_{13}, g_{14}, g_{21} and g_{22}, represent the MAI channel gains, which are inversely proportional to the distance squared. The users in example 1 can successfully reuse the subcarriers since the values of the intended user channel gains are stronger than the MAI channel gains, because the users are far from the interfering cell. In example 2, the subcarrier set reuse fails due to the strong MAI when the users are near the cell boundaries.

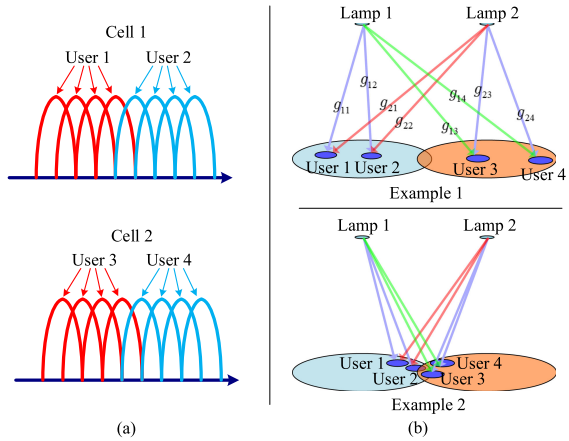

Fig. 5. Subcarrier reuse illustration showing (a) the subcarrier reuse scheme, and (b) two examples of user placements and their resulting channel gains.

For a general case, we assume there are Q LED lamps in a room serving Q cells. In each cell, K active users utilize the entire frequency range,[1] i.e., all subcarriers. In this paper, we assume all the subcarriers in each cell are available to be used. For the ℓth subcarrier of user k in cell q, we can derive the SINR as

$$\gamma_{qk\ell} = \frac{\frac{2N_k}{N^2}\rho^2\alpha_q^2 P_{\max}^2 |H_{qk}[\ell]|^2 c_{q\ell}^2}{\underbrace{\frac{2N_k}{N^2}\rho^2\alpha_q^2 P_{\max}^2 \sum_{i\neq q}^{Q} |H_{ik}[\ell]|^2 c_{i\ell}^2}_{\text{MAI}} + \frac{2N_k}{N}\sigma_{\text{clip},q}^2 + B_k\mathcal{N}_o}. \tag{10}$$

The data rate for user k located in the qth cell can be calculated as

$$R_b^{(qk)} = R_s \sum_{\ell\in S_k} \log_2 M_{q\ell}, \tag{11}$$

where $M_{q\ell}$ is the QAM modulation constellation size for the data modulated on the ℓth subcarrier, and the OFDM symbol rate is R_s. We assume all the users are synchronized. To maximizing

[1]In this paper, we assume all cell have exactly K users for the sake of notational simplicity.

the throughput fairness among users in the indoor space, the modulation index can be optimized. The objective function is given by

$$\max_{c_{q\ell},M_{q\ell},R_s} \min_{q,k,|S_k|} \sum_{\ell \in S_k} \log_2 M_{q\ell} R_s$$

$$\text{s.t.} \frac{\sqrt{M_{q\ell}}-1}{\sqrt{M_{q\ell}}\log_2\left(\sqrt{M_{q\ell}}\right)} \text{erfc}\left(\sqrt{\frac{3\gamma_{qk\ell}}{2(M_{q\ell}-1)}}\right) < B^{\max}$$

$$\forall\, \ell \in S_k,\ q = 1, 2, \ldots, Q, \text{ and } k = 1, 2, \ldots, K \tag{12}$$

where $B^{\max}$ is the maximum acceptable bit error rate, usually set to 10^{-4} with the help of forward error control (FEC) coding. The BER constraint shown in (12) guarantees data transmission reliability. The size of the subcarrier sets, $|S_k|\ \forall\, k$, are optimized, which requires integer optimization. The symbol rate, R_s, is also an optimization parameter, which is optimized to maximize the bit rate.

Solving the problem shown in (12) requires a nonlinear and non-convex optimization process. In this paper, we make several simplifications to make the computation feasible:

- It is not realistic to optimize the modulation index for each subcarrier due to the large computational burden. In this paper, we set the modulation indexes for all of a user's subcarriers the same, per cell; therefore, a smaller number of variables needs to be solved compared to optimizing the modulation index for each subcarrier separately.
- When a large N is used, the computational complexity of optimizing the assignment of each subcarrier to a user is prohibitive. Adjacent subcarriers can be banded and assigned as a set. For example, if $N = 512$, bands of 8 adjacent subcarriers can be assigned together. For most of the results in this paper, we further assume that the users are all assigned the same number of subcarrier bands. For a more general optimization process, the number of subcarriers for each user can be optimized. This optimization adds $K - 1$ optimization variables, which is significant if computational resources are constrained.
- In this work, we use a genetic algorithm (GA) as our heuristic to solve (12); GAs are powerful and effective at solving this type of problem [29], [30], but do not guarantee an optimal solution. Since GAs are well known classic heuristic searching methods, they are not described in this paper.

IV. Numerical Results

In this section, numerical results on the performance of the proposed OFDMA system are shown. Unless otherwise noted, the parameters used to obtain the results are given in Table II. The parameters used in this paper, such as the room dimension and locations of the LEDs, are typical for indoor spaces, and often used as a benchmark scenario in VLC research literature [31], [32]. The noise experienced at the receiver is assumed to be white, with spectral density calculated as in [33]. The testing environment is a 5 m × 5 m × 3 m empty room with 4 LED lamps, and each lamp serves one cell. The distance between lamps is denoted as L, which is a design parameter, as shown in Fig. 6. The users are assumed to have a bandwidth sufficient for the subcarriers assigned to them. The users are randomly located in each cell to evaluate the system performance fairly, and 50 trials of the users' locations are conducted, the channel gains of which are computed using (1). For the GA, 50 random initial individuals and up to 100 generations (iterations) are used for the optimization. The anti-aliasing low-pass filters at the receivers are assumed to be ideal.

TABLE II
Parameters Used for Numerical Results

Size of the small room	$5 \times 5 \times 3$ m^3
Number of LEDs, Q	4
Number of users per cell, K	up to 16
Number of subcarriers, N	512
Responsivity, ρ	0.5 A/W
Area of the photodetector, A	0.3 cm^2
Peak radiated optical power per lamp, $P_{\max}$	5 W
Noise spectral density	10^{-21} A^2/Hz
3 dB bandwidth of LEDs	20 MHz
Modulation constellation sizes	$2, 4, 8, 16, 32$
BER requirement, $B^{\max}$	10^{-4}

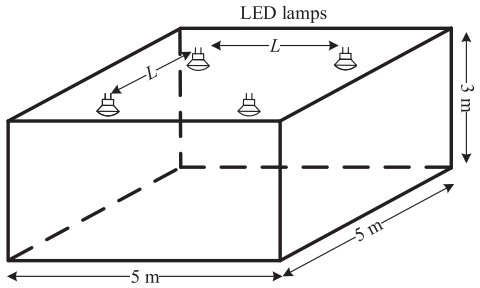

Fig. 6. Indoor environment with four cells used in the numerical results.

Fig. 7 shows the received power distribution and the status of reuse of the subcarriers in the room for two scenarios with different lamp spacings, $L = 1.7$ m and 3.3 m. At each point in the room, *subcarrier reuse* is a binary status value, 1 or 0, identifying the area where reuse can successfully be applied or not, respectively. A subcarrier cannot be reused either because the MAI is too strong or because of low lighting, both resulting in a low SINR. As seen in Fig. 7(a) for $L = 1.7$ m, the received optical power remains relatively uniformly distributed in the center of the room so that an acceptable illumination performance is achieved.[2] Due to MAI, the areas close to the boundaries between the cells cannot support subcarrier reuse, as shown in Fig. 7(b). The areas close to the walls and corners of the room are not usable due to the low illumination level. Fig. 7(c) shows the received optical power distribution when $L = 3.3$ m. In this case, the central part of the room is not well illuminated since the lamps are quite separate, and the beamwidth (the half-power full-angle of the LED) is not wide enough to illuminate the center of the room. Fig. 7(d) gives the reuse distribution for $L = 3.3$ m,

[2]Throughout this paper, the only illumination considered comes from the system's VLC-enabled LED lighting. Stricter illumination requirements can be satisfied by using other architectural lighting elements.

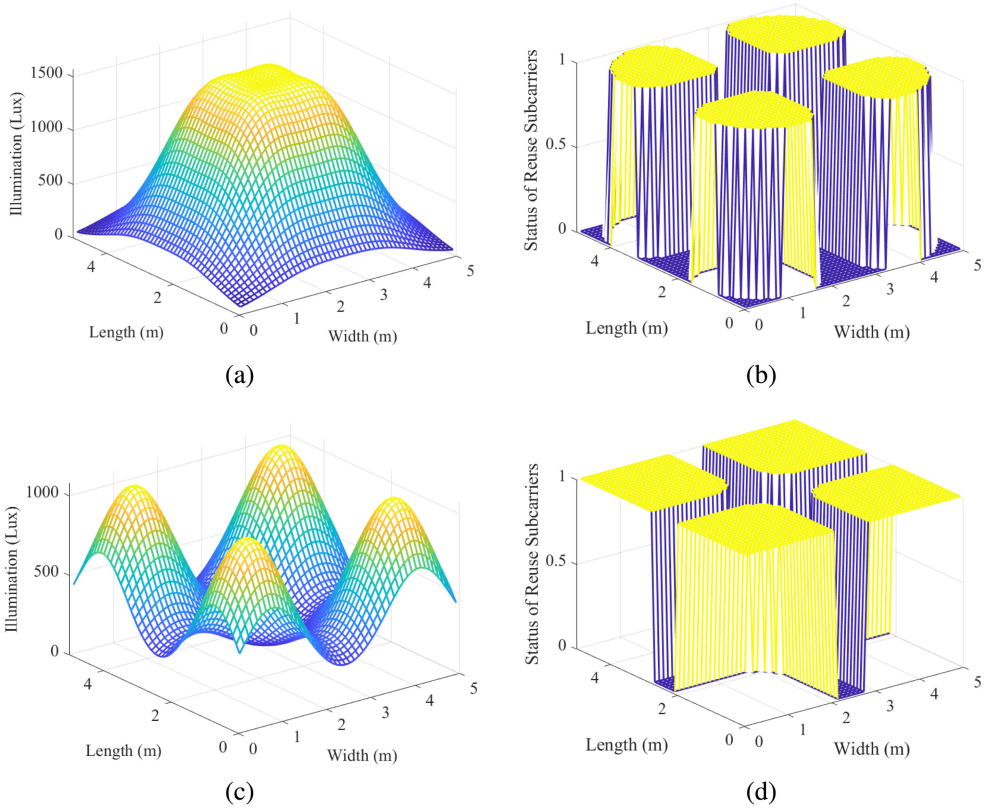

Fig. 7. Illustration of the received power and subcarrier reuse status in the room for an LED beamwidth of 80 degrees. (a) Received power distribution for $L = 1.7$ m. (b) Subcarrier reuse status for $L = 1.7$ m. (c) Received power distribution for $L = 3.3$ m. (d) Subcarrier reuse status for $L = 3.3$ m.

where the portions of the room where subcarrier reuse can occur clearly outline the center of each cell. In both Fig. 7(b) and (d), the center of the room cannot support subcarrier reuse due to strong MAI.

We define the subcarrier reuse probability as the frequency of subcarrier reuse, i.e., the probability that usable subcarriers are reused when multiple users are randomly located in each cell. Similarly, we define the coverage ratio as the fraction of the room that has at least 25 lux (10% of the standard illumination for offices, according to the Illuminating Engineering Society of North America [34]). Fig. 8 shows the reuse probability as well as the illumination coverage ratio as the distance between two lamps, L, increases. As predicted in Fig. 7, we see in Fig. 8 that the subcarrier reuse probability strongly depends on the locations of the LED lamps. When the LED beamwidth is 120 degrees, large enough to provide uniform illumination in the room, increasing the distance between the lamps improves the reuse probability since a larger distance between lamps results in a smaller MAI. For LED beamwidths of 40 or 80 degrees, as the distance between the lamps increases, the reuse probability improves at first due to the lower MAI. Further increasing L leads to a smaller illumination coverage area, and the reuse probability suffers because of the decreased SINR; some indoor spaces are simply not sufficiently illuminated, as seen on the right-hand axis of Fig. 8.

Fig. 9 shows the average per-user throughput as the number of users varies. For these results, subcarriers are assigned to users in multiples of 8. As expected, the average data rate decreases as

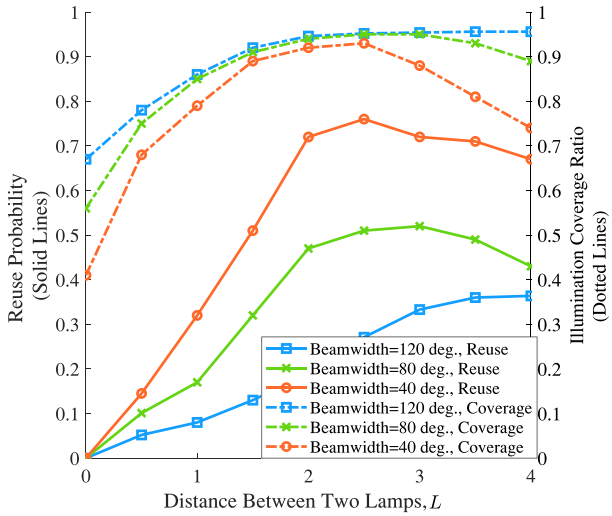

Fig. 8. Subcarrier reuse probability and illumination coverage as the distance between lamps varies for $K = 4$ users per cell.

the number of users increases. What we call the conventional scheme (does not use the multi-cell structure and optimizes the modulation index for each user) supports multiple users without using subcarrier reuse; thus, the number of subcarriers for each user decreases when more users need to be served. For the proposed multi-cell OFDMA scheme, the users that are supported in different cells can reuse the subcarriers to enhance their utilization efficiency due to the space diversity of the users.

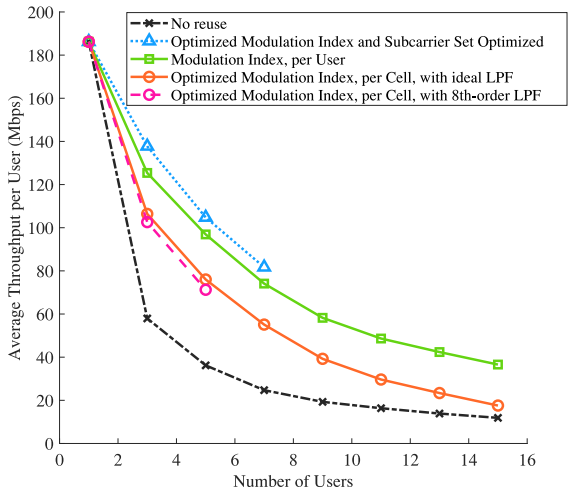

Fig. 9. Average throughput comparison of the proposed scheme and conventional OFDMA without subcarrier reuse.

Therefore, the average throughput using the proposed OFDMA scheme is substantially higher (about a factor of four) compared with the conventional scheme.

In this figure, we also compare the performance if the same modulation index is used for all the subcarriers in a cell versus optimizing the modulation indexes for each user. The algorithm that optimizes the modulation indexes for each user controls the transmitted power adaptively considering the peak power constraint. Since the magnitude of the channel frequency response rolls off as the frequency increases, optimizing the modulation indexes can maximize the overall throughput fairly, especially for users using the higher-frequency subcarrier sets. Using the parameters in this paper, systems that fix the modulation indexes within the cell only reach about half of the throughput compared with optimizing the modulation index for each user.

Fig. 9 also shows the throughput when the number of subcarriers assigned to each user is optimized, compared with the other cases that use the same number of subcarriers per user ($|S_k| = N/2\,K$). Since optimizing the number of subcarriers per user gives more freedom to utilize the spectrum resources better, the average optimized throughput is about 10% higher than setting the same number of subcarriers per user. This advantage comes at the cost of a more complex optimization problem.

In Fig. 9, we also test the ideal low-pass filter assumption by comparing the results to using a realistic anti-aliasing filter prior to sampling. An 8th-order Butterworth low-pass filter is applied to the case of optimizing the modulation index per cell. Compared with the results using an ideal low-pass filter, the 8th-order filter can suppress the adjacent subcarriers and provide almost identical performance.

V. Conclusion

In this paper, we propose a cellular OFDMA scheme for VLC systems to support multiple users based on DCO-OFDM. A comprehensive model of the system is provided, including filtering effects, power allocation, subcarriers allocation, frequency reuse, and clipping distortion. In the proposed scheme, sets containing adjacent subcarriers are assigned to users, allowing the users assigned low-frequency subcarriers to use a lower sampling rate and a smaller FFT; thus, the receiver's complexity and cost can be reduced. The modulation index for each user is optimized by maximizing the minimum throughput over the users, considering the peak radiation power constraint. The subcarrier reuse status across the room is illustrated for different scenarios and various system parameters. The subcarrier reuse probability for different LED's beamwidths is also presented. Compared with OFDMA without subcarrier reuse, the proposed scheme can provide about four times higher throughput for the system parameters and indoor space tested.

Appendix

This appendix verifies that after filtering the OFDM signal at the receiver, the sampling rate can be reduced to $2N_kR_s$ and a $2N_k$-FFT can be used for user k. For notational simplicity, we consider the noiseless case here. Assume that subcarrier ℓ has been assigned to user k in cell q. The estimate of the intended data modulated on the ℓth subcarrier in the qth cell when sampled at the full rate (NR_s) and using an N-FFT can be obtained as

$$\begin{aligned}\hat{X}_{q\ell} &= N\text{-FFT}(r_{qk}[n]) = \sum_{n=-N/2}^{N/2-1} r_{qk}[n]\exp\left(\frac{-j2\pi n\ell}{N}\right)\\ &= \alpha_q\rho\sum_{n=-N/2}^{N/2-1}(x_q[n]*h_{qk}[n])\exp\left(\frac{-j2\pi n\ell}{N}\right)\\ &= \alpha_q\rho|H_{qk}[\ell]|\sum_{n=-N/2}^{N/2-1} x_q[n]\exp\left(\frac{-j2\pi n\ell}{N}\right)\\ &\ell \in S_k \in \{0,1,\ldots,N_k-1\}. \end{aligned} \tag{13}$$

Sampling the received signal at $2N_kR_s$ is equivalent to downsampling the discrete signal by $\frac{N}{2N_k}$ when the sampling rate is NR_s. Therefore, we can substitute (2) into (13) and obtain

$$\begin{aligned}\hat{X}_{q\ell} &= \alpha\rho|H_{qk}[\ell]|\sum_{n=-N_k}^{N_k-1} x_q\left[n\frac{N}{2N_k}\right]\exp\left(\frac{-j2\pi n\ell}{2N_k}\right)\\ &= \alpha\rho|H_{qk}[\ell]|\sum_{n=-N_k}^{N_k-1}\left(\frac{1}{N}\sum_{\ell'=-N/2}^{N/2-1} c_{q\ell'}X_{q\ell'}\exp\left(\frac{j2\pi\ell'}{N}\frac{Nn}{2N_k}\right)\right)\\ &\quad \exp\left(\frac{-j2\pi\ell n}{2N_k}\right).\end{aligned} \tag{14}$$

Since a sharp low-pass filter is used, $X_{q\ell'} = 0$ for $|\ell'| >= 2N_k - 1$, and (14) is reduced to

$$\begin{aligned}\hat{X}_{q\ell} = \alpha\rho|H_{qk}[\ell]|\sum_{n=-N_k}^{N_k-1}\Bigg(\frac{1}{N}\sum_{\ell'=-N_k}^{N_k-1} c_{q\ell'}X_{q\ell'}\exp\left(\frac{j2\pi\ell'}{N}\frac{Nn}{2N_k}\right)\\ \exp\left(\frac{-j2\pi\ell n}{2N_k}\right)\Bigg)\end{aligned}$$

$$= \frac{1}{N}\alpha\rho|H_{qk}[\ell]| \sum_{n=-N_k}^{N_k-1} \sum_{\ell'=-N_k}^{N_k-1} c_{q\ell'} X_{q\ell'} \exp\left(\frac{j2\pi(\ell'-\ell)}{2N_k}\right)$$

$$= \alpha\rho\frac{2N_k}{N}|H_{qk}[\ell]|c_{q\ell}X_{q\ell}, \quad \ell \in S_k = \{0, 1, \ldots, N_k - 1\}. \tag{15}$$

Therefore, after the low-pass filter, the sampling rate for user k can be reduced to $2N_kR_s$, and a $2N_k$-FFT can be used for demodulation.

REFERENCES

[1] A. Jovicic, J. Li, and T. Richardson, "Visible light communication: opportunities, challenges and the path to market," *IEEE Commun. Mag.*, vol. 51, no. 12, pp. 26–32, Dec. 2013.

[2] T. Komine and M. Nakagawa, "Fundamental analysis for visible-light communication system using LED lights," *IEEE Trans. Consum. Electron.*, vol. 50, no. 1, pp. 100–107, Feb. 2004.

[3] V. A. Vilnrotter and M. Srinivasan, "Adaptive detector arrays for optical communications receivers," *IEEE Trans. Commun.*, vol. 50, no. 7, pp. 1091–1097, Jul. 2002.

[4] R. M. R. Mehmood, H. Elgala, and H. Haas, "Indoor MIMO optical wireless communication using spatial modulation," in *Proc. IEEE Int. Conf. Commun.*, May 2010, pp. 1–5.

[5] J. Lian and M. Brandt-Pearce, "Adaptive M-PAM for multiuser MISO indoor VLC systems," in *Proc. IEEE Global Commun. Conf.*, 2016, pp. 1–6.

[6] A. M. Abdelhady, O. Amin, A. Chaaban, B. Shihada, and M. Alouini, "Downlink resource allocation for dynamic TDMA-based VLC systems," *IEEE Trans. Wireless Commun.*, vol. 18, no. 1, pp. 108–120, Jan. 2019.

[7] Y. Qiu, S. Chen, H. Chen, and W. Meng, "Visible light communications based on CDMA technology," *IEEE Wireless Commun.*, vol. 25, no. 2, pp. 178–185, Apr. 2018.

[8] X. Bao, X. Zhu, T. Song, and Y. Ou, "Protocol design and capacity analysis in hybrid network of visible light communication and OFDMA systems," *IEEE Trans. Veh. Technol.*, vol. 63, no. 4, pp. 1770–1778, May 2014.

[9] B. Lin, X. Tang, Z. Ghassemlooy, C. Lin, and Y. Li, "Experimental demonstration of an indoor VLC positioning system based on OFDMA," *IEEE Photon. J.*, vol. 9, no. 2, pp. 1–9, Apr. 2017.

[10] Z. Chen and H. Haas, "Space division multiple access in visible light communications," in *Proc. IEEE Int. Conf. Commun.*, 2015, pp. 5115–5119.

[11] T. Little, M. Rahaim, I. Abdalla, E. Lam, R. Mcallister, and A. M. Vegni, "A multi-cell lighting testbed for VLC and VLP," in *Proc. Global LIFI Congr.*, 2018, pp. 1–6.

[12] H. Yang, C. Chen, W. Zhong, and A. Alphones, "Joint precoder and equalizer design for multi-user multi-cell MIMO VLC systems," *IEEE Trans. Veh. Technol.*, vol. 67, no. 12, pp. 11354–11364, Dec. 2018.

[13] V. Van Huynh, N. Le, N. Saha, M. Z. Chowdhury, and Y. M. Jang, "Inter-cell interference mitigation using soft frequency reuse with two FOVs in visible light communication," in *Proc. Int. Conf. ICT Convergence*, 2012, pp. 141–144.

[14] Y. Wang, X. Wu, and H. Haas, "Resource allocation in LiFi OFDMA systems," in *Proc. IEEE Global Commun. Conf.*, 2017, pp. 1–6.

[15] X. Ling, J. Wang, Z. Ding, C. Zhao, and X. Gao, "Efficient OFDMA for LiFi downlink," *J. Lightw. Technol.*, vol. 36, no. 10, pp. 1928–1943, May 2018.

[16] J. Lian and M. Brandt-Pearce, "Multiuser visible light communications using OFDMA," in *Proc. Eur. Conf. Opt. Commun.*, Sep. 2019, pp. 1–4.

[17] Y. Kim, T. Kwon, and D. Hong, "Area spectral efficiency of shared spectrum hierarchical cell structure networks," *IEEE Trans. Veh. Technol.*, vol. 59, no. 8, pp. 4145–4151, Oct. 2010.

[18] Y. Wang, L. Tao, Y. Wang, and N. Chi, "High speed WDM VLC system based on multi-band CAP64 with weighted pre-equalization and modified CMMA based post-equalization," *IEEE Commun. Lett.*, vol. 18, no. 10, pp. 1719–1722, Oct. 2014.

[19] K. Lee, H. Park, and J. R. Barry, "Indoor channel characteristics for visible light communications," *IEEE Commun. Lett.*, vol. 15, no. 2, pp. 217–219, Feb. 2011.

[20] L. Zeng *et al.*, "Equalisation for high-speed visible light communications using white-LEDs," in *Proc. 6th Int. Symp. Commun. Syst., Netw. Digit. Signal Process.*, Jul. 2008, pp. 170–173.

[21] J. Armstrong and A. J. Lowery, "Power efficient optical OFDM," *Electron. Lett.*, vol. 42, no. 6, pp. 370–372, Mar. 2006.

[22] S. D. Dissanayake and J. Armstrong, "Comparison of ACO-OFDM, DCO-OFDM, and ADO-OFDM in IM/DD systems," *J. Lightw. Technol.*, vol. 31, no. 7, pp. 1063–1072, Apr. 2013.

[23] N. Fernando, Y. Hong, and E. Viterbo, "Flip-OFDM for unipolar communication systems," *IEEE Trans. Commun.*, vol. 60, no. 12, pp. 3726–3733, Dec. 2012.

[24] J. Lian and M. Brandt-Pearce, "Clipping-enhanced optical OFDM for visible light communication systems," *J. Lightw. Technol.*, vol. 37, no. 13, pp. 3324–3332, Jul. 2019.

[25] M. Ergen, *Mobile Broadband:Including WiMAX and LTE*. Berlin, Germany: Springer, 2009.

[26] J. Armstrong, "OFDM for optical communications," *J. Lightw. Technol.*, vol. 27, no. 3, pp. 189–204, Feb. 2009.

[27] J. Bussgang, "Cross-correlation function of amplitude-distorted Gaussian signals," Res. Lab. Electron., Massachusetts Inst. Technol., Tech. Rep., vol. 216, Mar. 1952.

[28] M. Noshad and M. Brandt-Pearce, "Hadamard-coded modulation for visible light communications," *IEEE Trans. Commun.*, vol. 64, no. 3, pp. 1167–1175, Mar. 2016.

[29] J. Lian and M. Brandt-Pearce, "Joint optimal waveform design for multiuser VLC systems over ISI channel," in *Proc. IEEE Int. Conf. Commun.*, 2017, pp. 1–6.

[30] W. Banzhaf, P. Nordin, R. Keller, and F. Francone, *Genetic Programming: An Introduction*. New York, NY, USA: Elsevier, 1998.

[31] T. Komine and M. Nakagawa, "Fundamental analysis for visible-light communication system using LED lights," *IEEE Trans. Consum. Electron.*, vol. 50, no. 1, pp. 100–107, Feb. 2004.

[32] K. Lee, H. Park, and J. R. Barry, "Indoor channel characteristics for visible light communications," *IEEE Commun. Lett.*, vol. 15, no. 2, pp. 217–219, Feb. 2011.

[33] D. A. Basnayaka and H. Haas, "Design and analysis of a hybrid radio frequency and visible light communication system," *IEEE Trans. Commun.*, vol. 65, no. 10, pp. 4334–4347, Oct. 2017.

[34] M. Stanley Rea, *IESNA Lighting Handbook*, 9th ed, New York, NY, USA: Illum. Eng. Soc. North America, 2000.

Jie Lian (Member) received the B.S. degree from Northwestern Polytechnical University, China, and the M.S. and Ph.D. degree in electrical engineering from the University of Virginia, Charlottesville, VA, USA, in 2014 and 2017, respectively. From 2018-2019, he was a Research Associate with the University of Virginia. Currently, he is working as a tenure-track Associate Professor with Northwestern Polytechnical University. His current research interests include signal processing, wireless communications, optical communications, visible light communications and indoor positioning, and underwater optical wireless communications and sensing.

Maïté Brandt-Pearce (Senior Member, IEEE) is a Professor of electrical engineering and Vice Provost for faculty affairs with the University of Virginia (UVA). She joined (UVA) after receiving the Ph.D. degree in electrical engineering from Rice University, in 1993. Her research interests include free-space optical communications, visible light communications, nonlinear effects in fiber-optics, and cross-layer design of optical networks subject to physical layer degradations. Dr. Brandt-Pearce is the recipient of an NSF CAREER Award and an NSF RIA. She is a co-recipient of the Best Paper Awards at ICC 2006 and GLOBECOM 2012. She had served on the editorial board of IEEE TRANSACTION OF COMMUNICATIONS, IEEE COMMUNICATIONS LETTERS, IEEE/OSA JOURNAL OF OPTICAL COMMUNICATIONS and *Networks and Springer Photonic Network Communications*. She was a Jubilee Professor at Chalmers University, Sweden, in 2014. After serving as the General Chair of the Asilomar Conference on Signals, Systems & Computers in 2009, she served as the Technical Vice-Chair of GLOBECOM 2016. She is a member of Tau Beta Pi, Eta Kappa Nu, and a Senior Member of the IEEE. In addition to co-editing a book entitled *Cross-Layer Design in Optical Networks*, Springer Optical Networks Series, 2013, Prof. Brandt-Pearce has over two hundred technical publications.